

# Spectral reflectance and emissivity of man-made surfaces contaminated with environmental effects

**John P. Kerekes**, MEMBER SPIE  
Rochester Institute of Technology  
Chester F. Carlson Center for Imaging Science  
54 Lomb Memorial Drive  
Rochester, New York 14623  
E-mail: kerekes@cis.rit.edu

**Kristin-Elke Strackerjan**  
Aerospace Engineering Test Establishment  
P.O. Box 6550 Station Forces  
Cold Lake, Alberta  
T9M 2C6 Canada

**Carl Salvaggio**, MEMBER SPIE  
Rochester Institute of Technology  
Chester F. Carlson Center for Imaging Science  
54 Lomb Memorial Drive  
Rochester, New York 14623

**Abstract.** Spectral remote sensing has evolved considerably from the early days of airborne scanners of the 1960's and the first Landsat multispectral satellite sensors of the 1970's. Today, airborne and satellite hyperspectral sensors provide images in hundreds of contiguous narrow spectral channels at spatial resolutions down to meter scale and spanning the optical spectral range of 0.4 to 14  $\mu\text{m}$ . Spectral reflectance and emissivity databases find use not only in interpreting these images but also during simulation and modeling efforts. However, nearly all existing databases have measurements of materials under pristine conditions. The work presented extends these measurements to nonpristine conditions, including materials contaminated with sand and rain water. In particular, high resolution spectral reflectance and emissivity curves are presented for several man-made surfaces (asphalt, concrete, roofing shingles, and vehicles) under varying amounts of sand and water. The relationship between reflectance and area coverage of the contaminant is reported and found to be linear or nonlinear, depending on the materials and spectral region. In addition, new measurement techniques are presented that overcome limitations of existing instrumentation and laboratory settings. These measurements enable simulation of optical images with objects in the scene attributed with realistic surface reflectance and emissivity spectra. © 2008 Society of Photo-Optical Instrumentation Engineers. [DOI: 10.1117/1.3000433]

Subject terms: spectral reflectance; spectral emissivity; environmental effects; optical simulation; optical modeling; hyperspectral imaging.

Paper 080264R received Apr. 5, 2008; revised manuscript received Sep. 5, 2008; accepted for publication Sep. 6, 2008; published online Oct. 22, 2008.

## 1 Introduction

Spectral remote sensing has evolved considerably from the early days of airborne scanners of the 1960's and the first Landsat multispectral satellite sensors of the 1970's. Today, airborne and satellite hyperspectral sensors provide images in hundreds of contiguous narrow spectral channels at spatial resolutions down to meter scale and spanning the spectral range of 0.4 to 14  $\mu\text{m}$ .<sup>1-3</sup> These data find applications in land cover mapping,<sup>4</sup> agricultural crop assessment,<sup>5</sup> and target detection applications,<sup>6</sup> among others. While many of these applications involve supervised analysis, where the analyst interprets the data by selecting known training areas within the image and use those as prototypes to analyze the rest of image, increasing sophistication of the data has enabled the use of reference spectral libraries in the analysis.<sup>7</sup>

These spectral reflectance and emissivity databases capture the spectral absorption features and spectral trends useful in mapping materials in the analysis of spectral imagery, but they are also useful and, in fact, necessary for the forward simulation and modeling of spectroradiometric scenes. One such simulation model is digital imaging and remote sensing image generation (DIRSIG),<sup>8</sup> which has been developed over the past 20 years at the Rochester In-

stitute of Technology (RIT). DIRSIG is a first-principles physics-based simulation model that uses computer-aided design (CAD) descriptions of natural and man-made objects and performs ray tracing of all reflected and emitted radiation to produce radiometrically correct at-sensor spectral radiances for scenes spanning the 0.4- to 14- $\mu\text{m}$  spectral region. A key aspect of this model is the database of the necessary spectral reflectance and emissivity curves that attribute each facet of objects, as well as areas of the background surface. These material spectra are acquired from archival databases or measured with field spectrometers to accurately represent the reflectance or emittance characteristics of real surfaces.

While existing spectral reflectance and emissivity databases provide a wide range of materials and some variability associated with their sampled nature, the vast majority are for materials measured under ideal or pristine conditions. This is desirable from the point of view of capturing the data relevant for that material alone, so it can be used in spectral matching analysis techniques or to simulate scenes under ideal conditions. However, most real spectral images are of scenes where the objects are observed under nonideal conditions such as having been weathered, soiled, or wet due to recent rainfall.

This reality of typical scenes led to a recent effort to expand the capability of DIRSIG to simulate more realistic



**Fig. 1** Vehicle measurement setup (red circle indicates the location of the instruments). (Color online only.)

scenes that include these types of environmental effects.<sup>9</sup> This work presents the results of laboratory and field measurements conducted under that research. Section 2 describes characteristics of existing databases and summarizes related work in the measurement and modeling of contaminated surfaces. Section 3 presents the measurement techniques used in our research, including some new techniques necessary to overcome limitations of the instrumentation and laboratory environment. Section 4 presents the results of the field and laboratory measurements, while Sec. 5 provides a summary and discussion of these results.

## 2 Spectral Databases and Related Work

Most published spectral reflectance databases contain measurements of minerals, soils, or vegetation and were established for geological, agronomy, or agricultural applications. The ENVI remote sensing software (ITT Visual Information Solutions, Boulder, Colorado) provides a compilation of spectral reflectance libraries, including materials mentioned before plus a variety of man-made materials.<sup>10-16</sup> However, nearly all of these measurements were made in the laboratory or in the field under pristine conditions. That is, the material was dry and clean so that the measured reflectance was representative of solely that material.

Such pristine databases are appropriate for material identification or spectral unmixing applications, but they fail to capture the variability in reflectance that can arise in outdoor natural settings, and is necessary for realism in synthetic image generation applications. There has been some work in characterizing the effects of disturbances on soils<sup>17</sup> and measurements of the effects of thin layers of water,<sup>18</sup> but no previous work could be found that conducted a systematic study of the impact on spectra of environmental contaminants for several man-made surfaces.

## 3 Measurement Techniques

Measurements were made both in the field and in the laboratory. The field measurements were made to capture the real-world effects of surface particles (road dust) and water for a variety of civilian vehicles. The laboratory measurements were made under controlled conditions to study the effects on reflectance and emissivity of select man-made

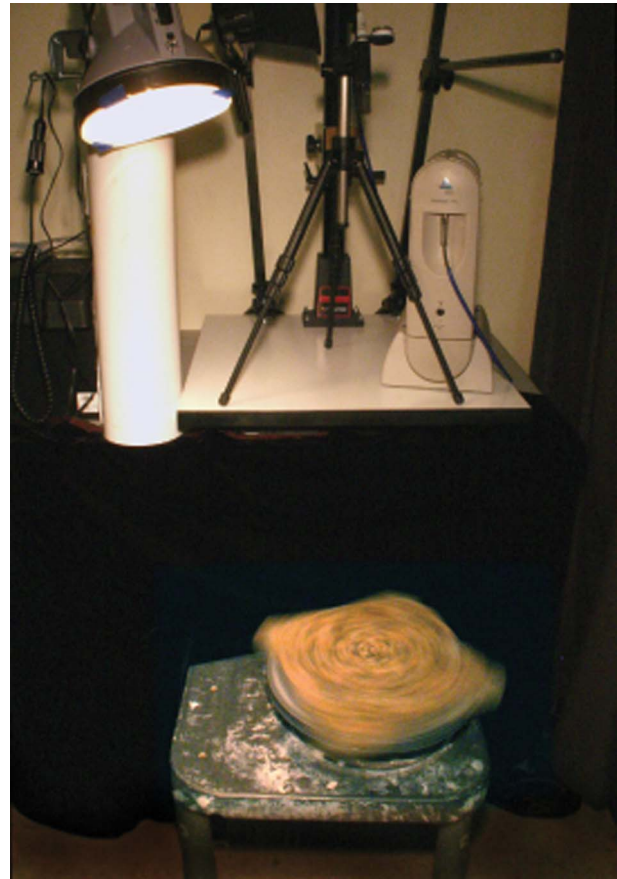


**Fig. 2** Laboratory setup for the ASD. The sample under test is blurred in this picture, as it rotates on the potter's wheel and temporally averaged spectra are collected.

materials for varying amounts of sand and water. Measurements in the reflective part of the spectrum (400 to 2500 nm) were made with an Analytical Spectral Devices (ASD) FieldSpec Pro (ASD, Incorporated, Boulder, Colorado), while the emissive measurements (8 to 14  $\mu\text{m}$ ) were made with a Designs and Prototypes (D&P) Instruments 102F FTIR Spectrometer (DP Instruments, Simsbury, Connecticut). The ASD was used with a

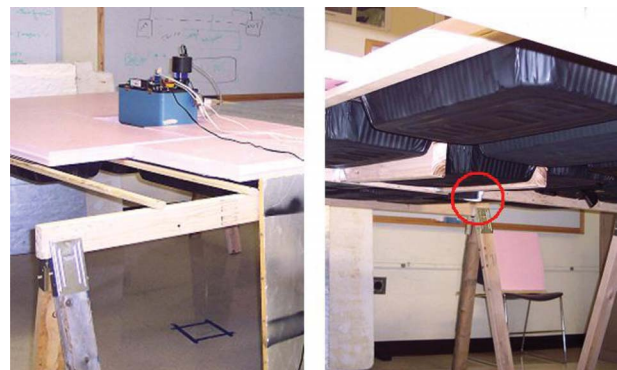


**Fig. 3** Laboratory setup for the D&P (the red circle indicates where the viewing port for the D&P was situated among the trays). (Color online only.)

**Table 1** General instrument configuration parameters for the spectrometers used in this study.

Parameter	ASD Field Spec Pro	D&P Instruments Model 102F microFTIR
Spectral range	0.35 to 2.5 $\mu\text{m}$	2.0 to 16.0 $\mu\text{m}$
Spectral resolution (FWHM)	<ul style="list-style-type: none"> <li>• 3 nm at 0.7 <math>\mu\text{m}</math></li> <li>• 10 nm at 1.4 <math>\mu\text{m}</math></li> <li>• 10 nm at 2.1 <math>\mu\text{m}</math></li> </ul>	4 $\text{cm}^{-1}$ at 2 $\mu\text{m}$ , 1 sec/scan
Spectral sampling	<ul style="list-style-type: none"> <li>• 1.4 nm from 0.35 to 1.0 <math>\mu\text{m}</math></li> <li>• 2 nm from 1.0 to 2.5 <math>\mu\text{m}</math></li> </ul>	4 $\text{cm}^{-1}$
Noise equivalent delta radiance	<ul style="list-style-type: none"> <li>• <math>1.4 \times 10^{-6}</math> W/cm<sup>2</sup>/sr/<math>\mu\text{m}</math> at 0.7 <math>\mu\text{m}</math></li> <li>• <math>2.4 \times 10^{-6}</math> W/cm<sup>2</sup>/sr/<math>\mu\text{m}</math> at 1.4 <math>\mu\text{m}</math></li> <li>• <math>8.8 \times 10^{-6}</math> W/cm<sup>2</sup>/sr/<math>\mu\text{m}</math> at 2.1 <math>\mu\text{m}</math></li> </ul>	n/a

Lambertian reflectance standard (Spectralon<sup>TM</sup>), which was used to convert the sample radiance to reflectance. The D&P was used with a gold standard and temperature probe to convert the sample radiance to emissivity. General instrument configuration parameters are listed in Table 1, and detailed discussions on the theory and protocols for these measurements are available on the website for the RIT Optical Properties Laboratory.<sup>19</sup> The following describes the specific measurement techniques used in this research in field and laboratory settings.

### 3.1 Field Measurements of Vehicles

To ensure the instruments had a clear nadir view of the painted surfaces of the vehicles, a scaffold was constructed and the instruments secured on a tripod overhanging the platform (Fig. 1). The scaffold was located on the opposite side of the vehicle from the sun, and care was taken to minimize reflective or emissive adjacency contributions from the scaffold and platform. Also, the measurements were made near local noon with the sun at high solar elevation angles (>70 deg). Data were collected with both the ASD and the D&P of the vehicles in four states: 1. dirty and dry (as arrived), 2. dirty and wet, 3. clean and wet, and 4. clean and dry. Tap water applied using spray bottles was used to wet down the paint surfaces to simulate wet conditions after a rain storm. The ASD and D&P measurements were made as quickly as possible (within minutes) to minimize any differences in the amount of water on the surface.

### 3.2 Laboratory Measurements of Reflectance

Measurements of several man-made materials with varying levels of environmental contaminants (described in Sec. 4) were made in the laboratory. An artificial light source was used to illuminate the materials for the measurement. In addition, due to the heterogeneous nature of the surfaces being measured and design characteristics of the ASD spectrometer, an innovative measurement setup was devised.

The ASD uses a fiber optic bundle to transmit light from the input optics to the spectrometer detectors. Separate subsets of the fibers lead to the different detectors required to span the full spectral range covered by the instrument. Thus, when observing heterogeneous surfaces, this design can lead to discontinuities in the measured spectrum, since the different detectors are actually observing different areas on the surface. This problem was overcome by the innovative use of a “potter’s wheel” to rotate the sample under test and temporally average the spectra (Fig. 2).

### 3.3 Laboratory Measurements of Emissivity

The theory for measuring the emissivity of materials requires a thermal contrast between the material surface under test and the background or “sky” irradiance. In the field this is commonly satisfied under clear conditions where the downwelling sky irradiance is very small compared to the surface emitted radiance. In our laboratory measurements we created an artificial cold sky through the use of ice-filled, pans painted black with insulating foam above. Figure 3 shows these pans suspended from a wood frame on sawhorses and providing a cold sky for materials placed on the floor for measurement. In addition, the samples under test were often also heated to provide additional contrast. It should be noted that emissivity measurements of highly reflective materials (low emissivity) are problematic both in the field as well as in the laboratory configuration presented in this work. From individual measurements of sample leaving spectral radiance  $L_{\text{sample}}(\lambda)$  and downwelling sky spectral radiance  $L_{\text{downwelling}}(\lambda)$ , one can compute the spectral emissivity as

$$\varepsilon_{\text{sample}}(\lambda) = \frac{L_{\text{sample}}(\lambda) - L_{\text{downwelling}}(\lambda)}{L_{\text{BB}}(\lambda, T_{\text{sample}}) - L_{\text{downwelling}}(\lambda)}, \quad (1)$$

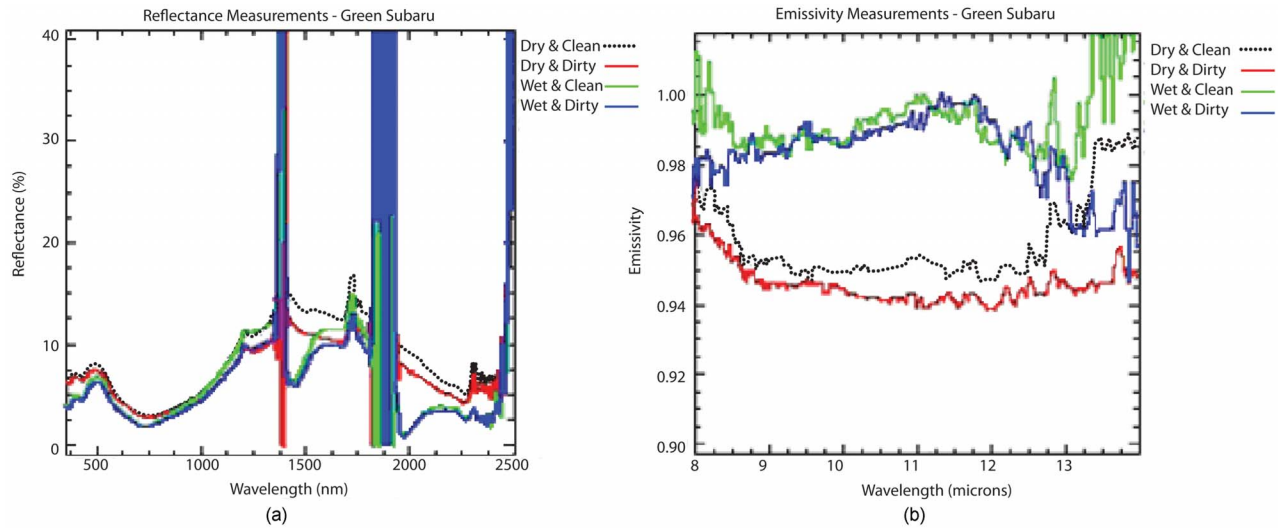


Fig. 4 Green Subaru—ASD reflectance spectra (a); D&P emissivity spectra (b).

where  $L_{BB}(\lambda, T_{\text{sample}})$  is the spectral radiance emitted from a blackbody at temperature  $T$ , computed using the Planck blackbody radiation equation. Measurement problems arise in two situations. The first is when the spectral downwelling radiance and the blackbody radiance are close in magnitude, for example, when the sky is not “severe clear.” This situation causes a mathematical instability in Eq. (1) as the denominator approaches zero at certain wavelengths, especially near atmospheric gas absorption lines. The second problem arises when the same situation occurs in the numerator of Eq. (1), when the sample leaving radiance, which is a function of both the sample temperature and emissivity, is low and close in magnitude to the downwelling sky radiance. This most often occurs for material

samples with low emissivity values (0.4 or less). Sensor noise will begin to play a dominant role in this situation.

The ice-filled tray approach presented in this work can only achieve background “sky” radiance values equivalent to a blackbody at 273 K. This is significantly higher than typical clear sky conditions observed outdoors, where the equivalent sky temperature is usually in the 240 to 260 K range. As a result, this technique imposes a tighter limitation on the range of emissivity values that may be successfully measured using a technique based on Eq. (1). While the lower limit has not been established as a part of this study, it is expected that materials with spectral emissivity values less than 0.5 will begin to pose problems.

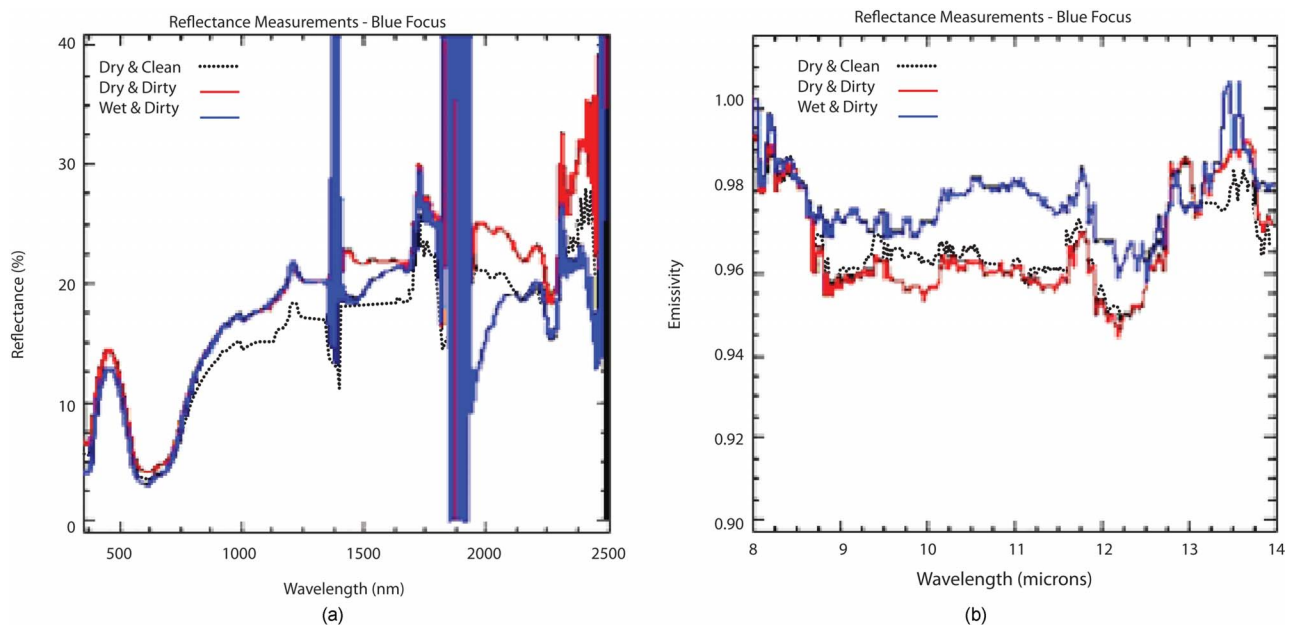


Fig. 5 Blue Ford—ASD reflectance spectra (a); D&P emissivity spectra (b).

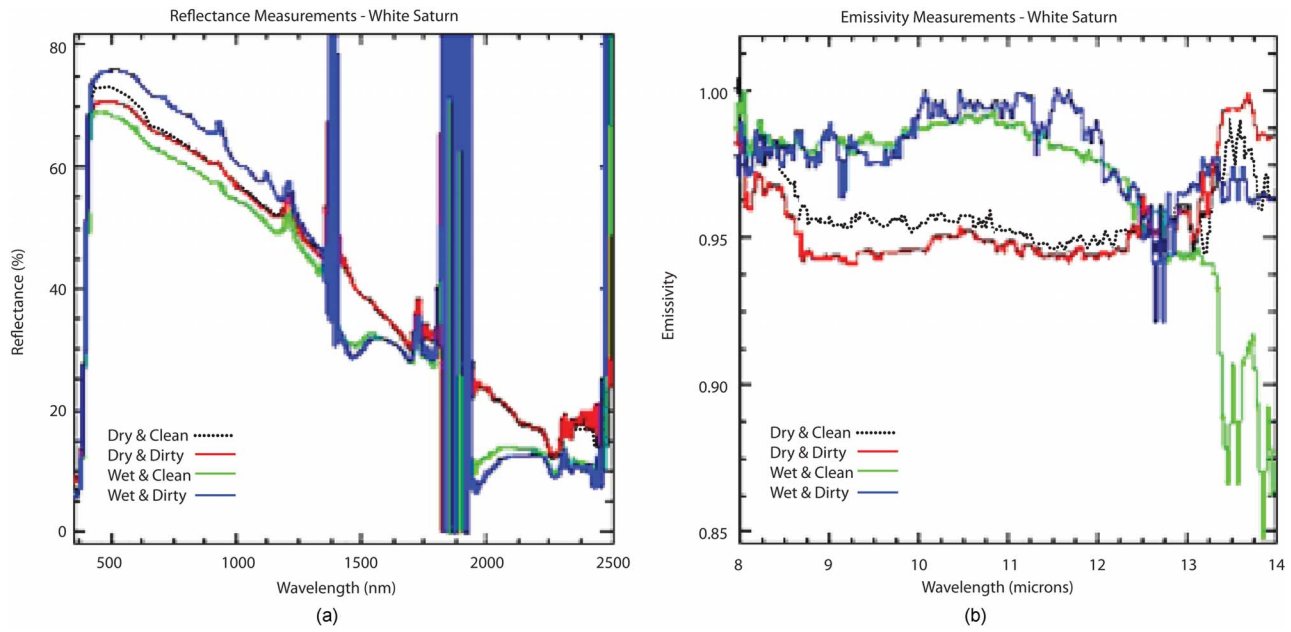


Fig. 6 White Saturn—ASD reflectance spectra (a); D&P emissivity spectra (b).

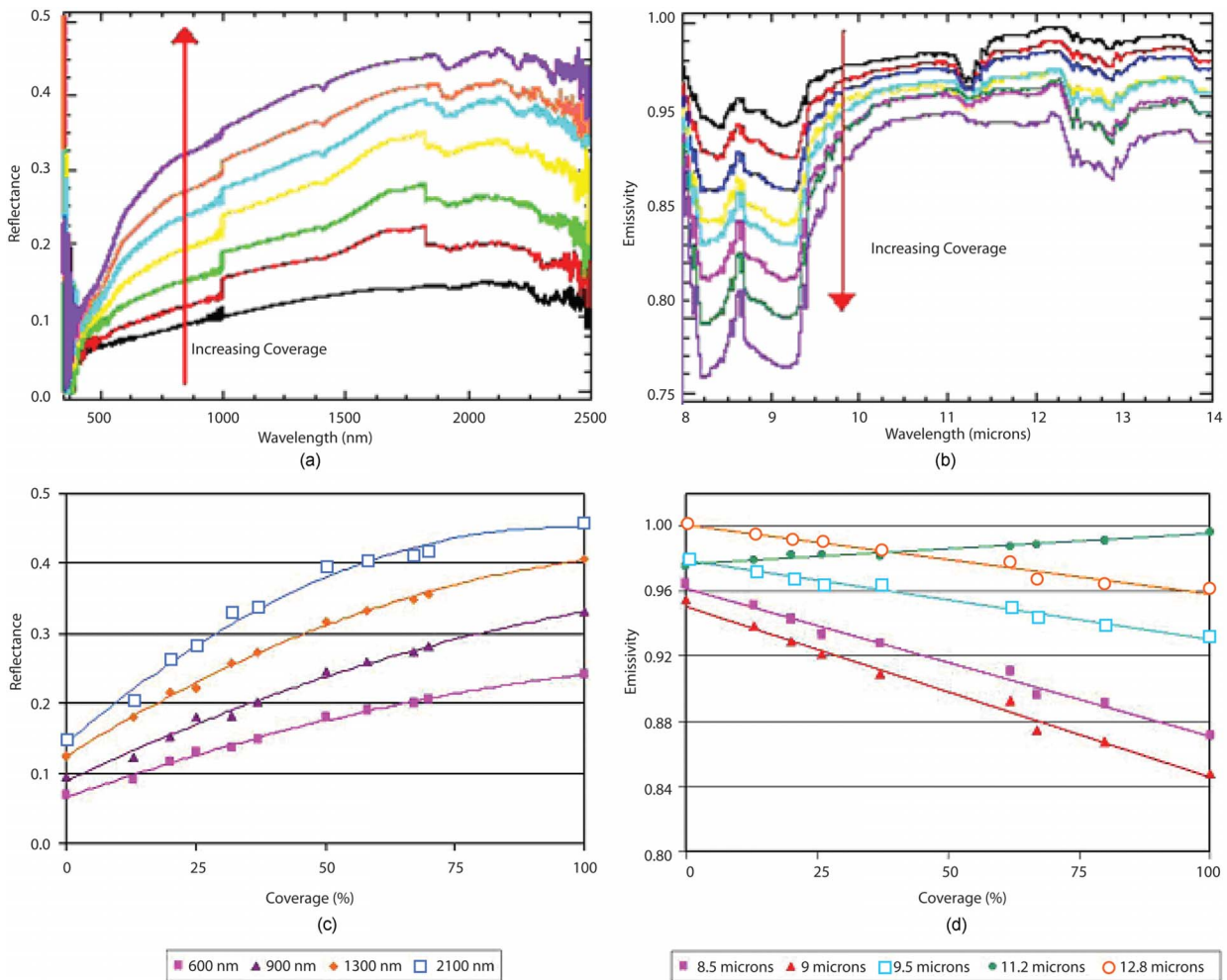
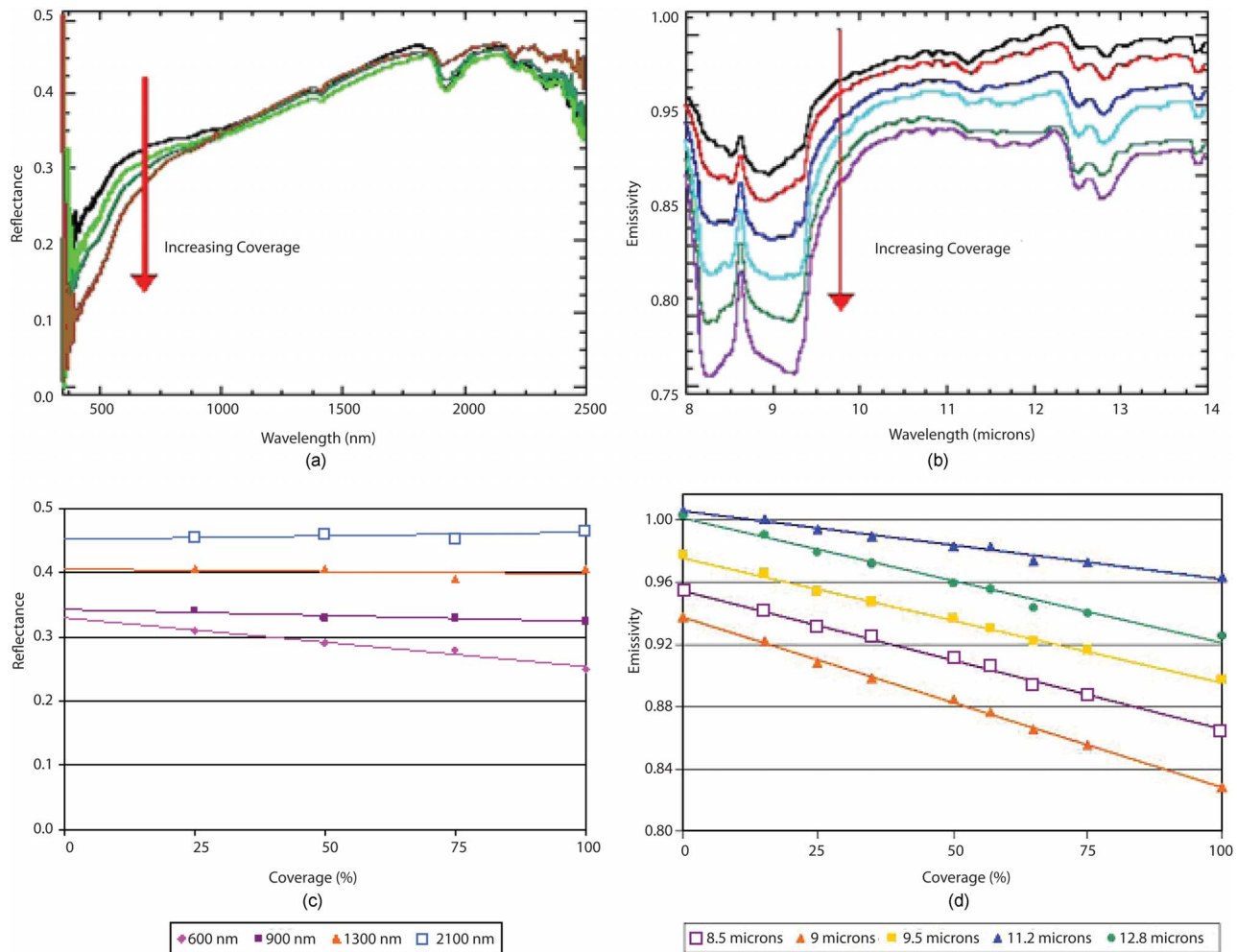


Fig. 7 Asphalt and sand. Reflectance (a) and emissivity (b) spectra with increasing coverage of the contaminant. Reflectance (c) and emissivity (d) at selected wavelengths as a function of area coverage of the contaminant.



**Fig. 8** Concrete and sand. Reflectance (a) and emissivity (b) spectra with increasing coverage of the contaminant. Reflectance (c) and emissivity (d) at selected wavelengths as a function of area coverage of the contaminant.

## 4 Results

The following sections present measured reflectance and emissivity spectra for vehicles collected in the field as well as for the various materials studied in the laboratory.

### 4.1 Spectra from Field Measurements of Vehicles

Results are presented for measurements of three vehicles: a blue Ford, a green Subaru, and a white Saturn. Figures 4–6 present the measured reflectance and emissivity spectra of these vehicles under the various surface contaminant conditions. No measurements under the wet and clean condition for the blue Ford were performed.

Several features are obvious in these measured spectra. In the visible (400 to 700 nm), the blue and green reflectance peaks, as well as the broad high reflectance for the white vehicle, demonstrate that visual colors persist under all surface conditions. With the exception of the wet and dirty condition for the white vehicle, all wet condition measurements showed a decrease in the reflectance in the visible. In the reflective infrared (700 to 2500 nm), the decrease in reflectance with the presence of water was

uniformly present in all cases. The decrease was most pronounced near the atmospheric water vapor absorption bands at 1400 and 1900 nm.

The same trend of a decrease in reflectance is seen in the thermal infrared (8 to 14  $\mu\text{m}$ ) plots, except it is shown as an increase in surface emissivity (1–reflectance). No particular surface water features are obvious in this part of the spectrum.

The effect of road dust on the surface reflectance and emissivity is less obvious, but in most cases resulted in a slight increase of the reflectance (except for the white vehicle) and a corresponding decrease in emissivity. The overall magnitude of the change due to the presence of road dust was seen to be less than the magnitude change due to the presence of water.

### 4.2 Spectra from Laboratory Measurements of Man-Made Materials

While the field measurements were useful to understand typical effects in the real world, the specific amounts of contaminants present were not controllable. Thus, measure-

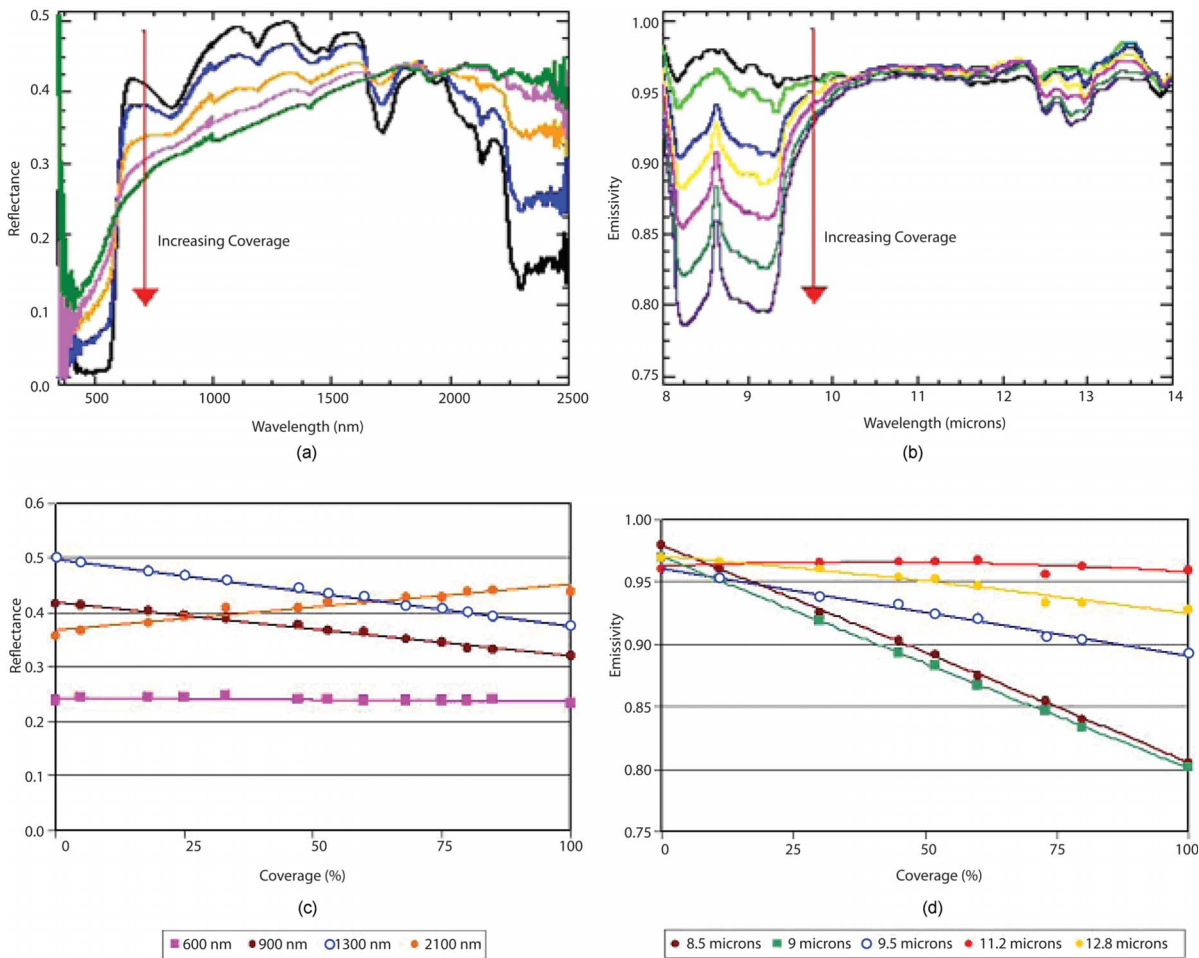


**Fig. 9** Red painted metal and sand. Reflectance (a) and emissivity (b) spectra with increasing coverage of the contaminant. Reflectance (c) and emissivity (d) at selected wavelengths as a function of area coverage of the contaminant.

ments were also made in the laboratory for several materials in a setting where the amount of contaminant could be quantified. Table 2 lists the materials and their contaminants measured in the laboratory. Measurements of water on the red painted metal and roofing shingle were not possible due to the spinning wheel technique used for the reflectance.

Figures 7–12 show the results of these measurements. In each figure we present both the spectra measured as the amount of the contaminant is varied, as well as the trend as a function of area coverage for selected wavelengths.

**Table 2** Materials and contaminants measured in the laboratory.

Material	Contaminant
Asphalt	Sand, water
Concrete	Sand, water
Red painted metal	Sand
Roofing shingle	Sand

In Fig. 7–10, we present the effect of sand on the various surfaces. In the reflective domain, we see the gradual transition from the spectral reflectance of the pure surface to the reflectance of sand. In some cases, there is a slight nonlinearity in the reflectance as a function of area sand coverage. This could indicate that some intimate mixing is occurring between the sand particles and the surface. In the emissive part of the spectrum, we see linear trends and a decrease in emissivity as more sand covers the surface.

Figures 11 and 12 present the effects of adding water on the surface. In all cases we see that the reflectance (and emissivity) has a nonlinear relationship with area coverage. It is seen to require only a very small amount of water to decrease the reflectance (or increase emissivity). This is consistent with our everyday experience in the visible part of the spectrum, where damp surfaces tend to be darker than dry surfaces. In the reflective, we see the deepening of the water absorption bands at 1400 and 1900 nm as the surface coverage increases.

In the upper right plots of Fig. 11 and 12, we see an interesting phenomenon that was not anticipated and to date has eluded explanation. For both surfaces, the emissivity in the 11.5- to 14- $\mu\text{m}$  range starts out relatively high, and

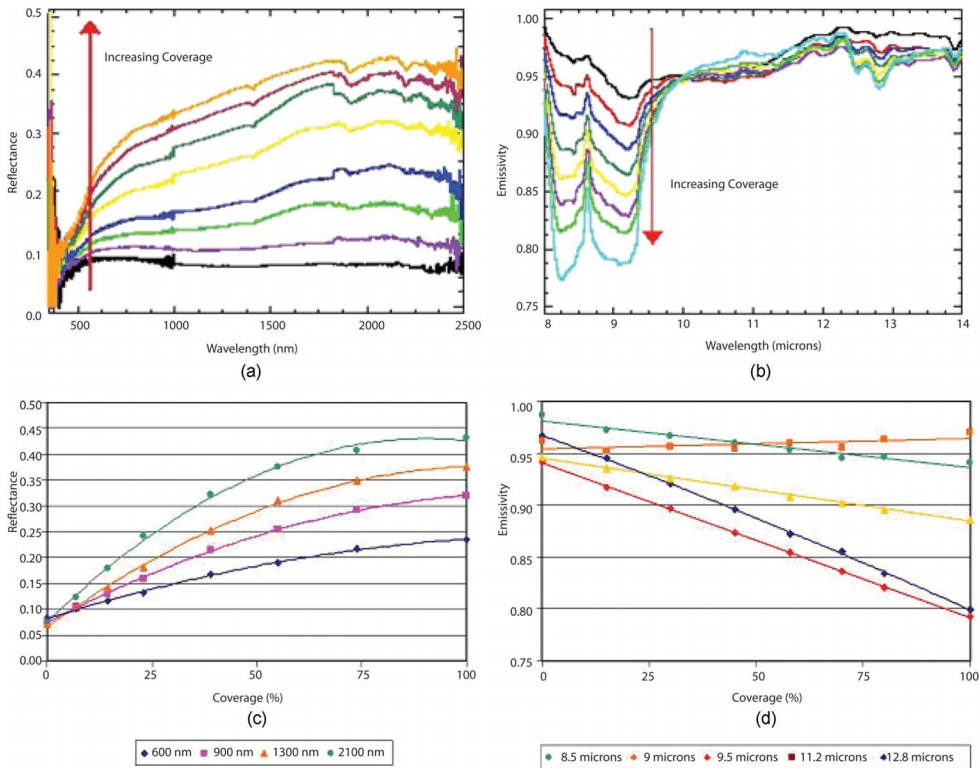


**Fig. 10** Roofing shingle and sand. Reflectance (a) and emissivity (b) spectra with increasing coverage of the contaminant. Reflectance (c) and emissivity (d) at selected wavelengths as a function of area coverage of the contaminant.

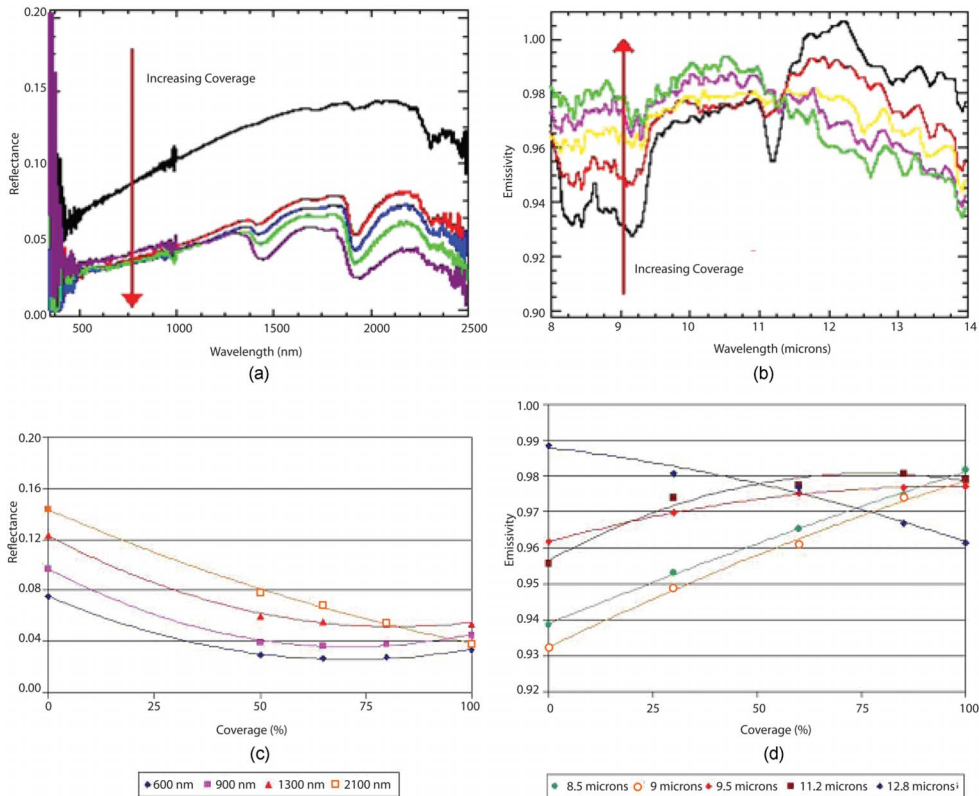


**Fig. 11** Asphalt and water. Reflectance (a) and emissivity (b) spectra with increasing coverage of the contaminant. Reflectance (c) and emissivity (d) at selected wavelengths as a function of area coverage of the contaminant.

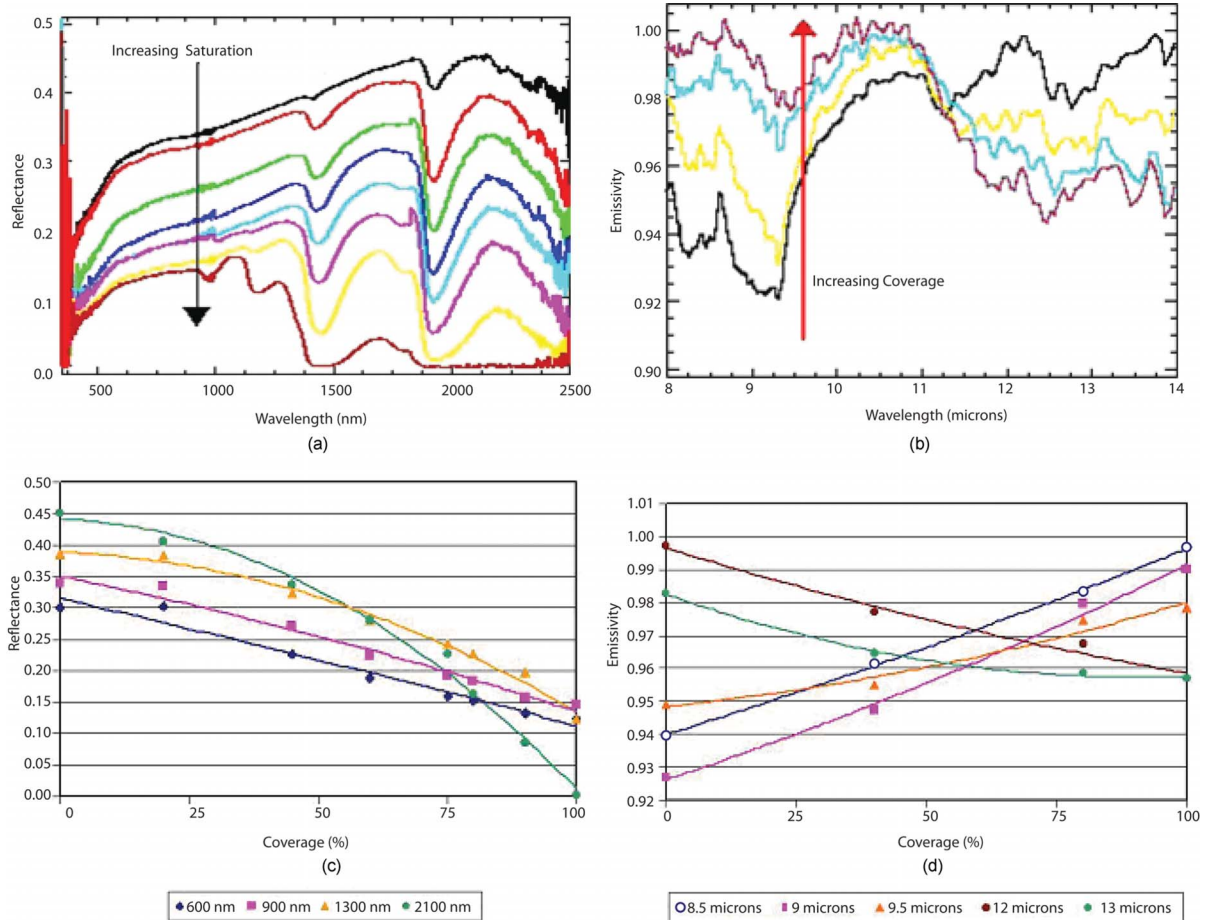


**Fig. 12** Concrete and water. Reflectance (a) and emissivity (b) spectra with increasing coverage of the contaminant. Reflectance (c) and emissivity (d) at selected wavelengths as a function of area coverage of the contaminant.

then decreases with increasing water coverage, a trend opposite that observed in the 8- to 11.5- $\mu\text{m}$  range and opposite to that expected from theory. Several attempts were made to remeasure the emissivity spectra under these conditions, and the results were very repeatable and consistent.

Since these results were repeatable, it is believed that there was a systematic unknown condition in the measurements conducted, most likely phenomenology that was introduced due to experimental techniques that modified the expected results. One hypothesis was that a humid microclimate was set up between the sample and the instrument aperture/cold background. In an attempt to increase thermal contrast between the target and the cold background, as stated previously, the sample material was heated. This likely resulted in increased evaporation of the water contaminant on the surface, increasing the water vapor content in the intervening optical path.

Since the measurements were made over time with decreasing water content on the surface, two things occurred during the measurement period. First the rate of increase of the water vapor in the localized microclimate slowed, and the material decreased in temperature due to both radiative cooling as well as cooling due to evaporative processes on the surface. The increased water vapor content may have resulted in small differential changes in transmission and

path radiance across the LWIR region as the experimental period proceeded. Second, there was a non-negligible decrease in sample temperature during the measurement period of several degrees K that resulted in a slight shift in the peak of the blackbody curve. In an attempt to mitigate the localized microclimate, ventilation was put in place; however, no change in the resulting emissivity spectra was observed. These anomalous results are included here for future researchers to possibly duplicate and/or explain.

## 5 Summary and Discussion

Laboratory and field measurements have been presented for the spectral reflectance and emissivity of various surface contaminants on common man-made materials. This study was motivated by an interest in the forward simulation of high resolution hyperspectral imagery of scenes that are more realistic than those that only use pristine measurements for surface reflectance or emissivity. Measurements of several vehicle paints were made in the field to obtain realistic but uncontrolled spectra, while measurements of additional surfaces were also made in the laboratory under more controlled conditions.

These measurements confirmed anticipated trends from mixing models with small amounts of sand leading to both

linear and nonlinear trends, depending on the underlying material surface. For a thin layer of water, nonlinear trends with water amounts were observed in all cases considered. One anomalous trend with a decrease in emissivity in the 11.5- to 14- $\mu\text{m}$  range with increasing water was observed and which to date has defied explanation. This result is reported here for future researchers to explore.

These data will be used in forward simulations of high resolution hyperspectral images of urban scenes to provide more realistic conditions (and variability) for surface materials. We are pursuing two approaches to use these data to implement this feature. One is the direct use of the spectra for contaminated surfaces of the materials as measured. The second is through the use of interpolation between the measured contamination coverage areas, which will allow the user to specify an arbitrary coverage amount. In addition, current research is investigating the use of first-principles particle scattering methods to generate reflectance spectra under a wide range of conditions. These data will be used for the validation of those spectra. Further work will also involve the measurement of additional materials and contaminants under varying illumination and viewing angles to better understand the goniometric effects of the contaminants.

## References

1. J. Pearlman, C. Segal, L. Liao, S. Carman, M. Folkman, B. Browne, L. Ong, and S. Ungar, "Development and operations of the EO-1 hyperion imaging spectrometer," *Proc. SPIE* **4135**, 43–253 (2000).
2. T. Cocks, R. Jenssen, A. Stewart, I. Wilson, and T. Shields, "The HyMap airborne hyperspectral sensor: the system, calibration, and performance," *Proc. 1st EARSEL Workshop on Imaging Spectroscopy*, Zurich, pp. 37–42 (1998).
3. J. Hackwell, D. Warren, R. Bongiovanni, S. Hansel, T. Hayhurst, D. Mabry, M. Sivjee, and J. Skinner, "LWIR/MWIR imaging hyperspectral sensor for airborne and ground-based remote sensing," *Proc. SPIE* **2819**, 102–107 (1996).
4. W. Zhang and S. Sriharan, "Using hyperspectral remote sensing for land cover classification," *Proc. SPIE* **5655**, 261–270 (2005).
5. B. C. Gao and A. Goetz, "Retrieval of equivalent water thickness and information related to biochemical components of vegetation canopies from AVIRIS data," *Remote Sens. Environ.* **52**(3), 155–162 (1995).
6. D. Manolakis and G. Shaw, "Detection algorithms for hyperspectral imaging applications," *IEEE Signal Process. Mag.* **19**(1), 29–43 (2002).
7. P. Lucey, M. Winter, E. Winter, and D. Steutel, "Automated material map generation using hyperspectral data: a case study using AVIRIS imagery," *Proc. SPIE* **4725**, 140–147 (2002).
8. J. R. Schott, S. D. Brown, R. V. Raqueno, H. N. Gross, and G. Robinson, "An advanced synthetic image generation model and its application to multi/hyperspectral algorithm development," *Can. J. Remote Sens.* **25**(2), 99–111 (1999).
9. K. Strackerjan, "Modelling the spectral effects of water and soil as surface contaminants in a high resolution optical image simulation," MS Thesis, Chester F. Carlson Center for Imaging Science, Rochester Institute of Technology, Rochester, New York (2006).
10. C. I. Grove, S. J. Hook, and E. D. Paylor, "Laboratory reflectance spectra for 160 minerals 0.4–2.5 micrometers," JPL Report 92–2, Jet Propulsion Laboratory, Pasadena, CA (1992).
11. A. R. Korb, P. Dybwad, W. Wadsworth, and J. W. Salisbury, "Portable FTIR spectrometer for field measurements of radiance and emissivity," *Appl. Opt.* **35**, 1679–1692 (1996).
12. J. W. Salisbury, D. M. D'Aria, and E. Jarosevich, "Midinfrared (2.5–13.5 micrometers) reflectance spectra of powdered stony meteorites," *Icarus* **92**, 280–297 (1991).
13. J. W. Salisbury, A. Wald, and D. M. D'Aria, "Thermal-infrared remote sensing and Kirchhoff's Law I. Laboratory measurements," *J. Geophys. Res.* **99**, 11,897–11,911 (1994).
14. J. W. Salisbury, L. S. Walter, N. Vergo, and D. M. D'Aria, *Infrared (2.1–25 micrometers) Spectra of Minerals*, Johns Hopkins University Press, Baltimore, MD, 1991.
15. R. N. Clark, G. A. Swayze, A. J. Gallagher, T. V. V. King, and W. M. Calvin, "The U.S. Geological Survey, Digital Spectral Library: Version 1: 0.2 to 3.0 microns," U. S. Geological Survey Open File Report 93–592 (1993); [http://speclab.cr.usgs.gov/spectral.lib04/clark1993/spectral\\_lib.html](http://speclab.cr.usgs.gov/spectral.lib04/clark1993/spectral_lib.html).
16. C. D. Elvidge, "Visible and infrared reflectance characteristics of dry plant materials," *Int. J. Remote Sens.* **11**(10), 1775–1795 (1990).
17. J. R. Johnson, P. G. Lucey, K. A. Horton, and E. M. Winter, "Infrared measurements of pristine and disturbed soils: 1. Spectral contrast differences between field and laboratory data," *Remote Sens. Environ.* **64**, 34–46 (1998).
18. H. J. Mitchell and C. Salvaggio, "MWIR and LWIR spectral signatures of water and associated materials," *Proc. SPIE* **5093**, 195–205 (2003).
19. RIT/CIS/DIRS Optical Properties Laboratory Protocols Library, see [http://dirs.cis.rit.edu/optical\\_properties\\_lab/protocols](http://dirs.cis.rit.edu/optical_properties_lab/protocols).



**John P. Kerekes** received his BS, MS, and PhD degrees in electrical engineering from Purdue University in 1983, 1986, and 1989, respectively. From 1989 to 2004 he was employed as a member of the technical staff at the Massachusetts Institute of Technology's Lincoln Laboratory, where he performed research and development in the modeling and analysis of optical and microwave remote sensing systems. Since 2004 he has been employed as an associate professor in the Chester F. Carlson Center for Imaging Science at the Rochester Institute of Technology. His research interests continue to be in the development and use of spectral imaging and other remote sensing technologies for the extraction of information from remotely sensed measurements. He is a senior member of the IEEE, and a member of SPIE, OSA, AGU, ASPRS, and AMS.



**Kristin-Elke Strackerjan** joined the Regular Officer Training Program (ROTP) in 1994 and attended Dalhousie University, where she completed her BS degree in 1998. On completion, she was commissioned as an officer in the Canadian Forces. In 1999 she attended Dalhousie once again and received her Diploma of Meteorology. From 2000 onward she has worked as an aerospace engineer in the Canadian Air Force. While in Ottawa, Ontario, from 2001 to 2004, she was part of the Maritime Helicopter Project. From 2004 to 2006 she attended the Rochester Institute of Technology, where she completed her MS in imaging science. She is currently posted to the Aerospace Engineering and Test Establishment at 4 Wing Cold Lake in Cold Lake, Alberta, where she is the imaging officer.



**Carl Salvaggio** received his BS and MS degrees in imaging science from the Rochester Institute of Technology (RIT) in 1987. He received his PhD in environmental resource engineering in 1994 from the State University of New York, College of Environmental Science and Forestry, at Syracuse University. From 1987 to 1994 he was a research scientist in the Digital Imaging and Remote Sensing Laboratory at RIT, where he developed scene simulation models, atmospheric correction and normalization algorithms, and image fusion techniques. From 1994 to 2002 he worked for the defense intelligence community developing and deploying ground truth experiments for model validation and spectral database development. Since 2002 he has been an associate professor in the Center for Imaging Science at RIT, developing novel optical properties measurement techniques as well as simulation of thermal infrared image phenomenology. He is a member of the SPIE and an associate member of the IEEE.